The order affects the release of vitamin D from hybrid self-assembled silica systems

Heliyon 10 (2024) e36080

Contents lists available at ScienceDirect

Heliyon

journal homepage: www.cell.com/heliyon

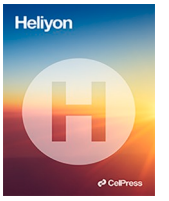

Research article

The order affects the release of vitamin D from hybrid self-assembled silica systems

Marta Gallo *, Mauro Banchero, Vittoria Cerbella, Silvia Ronchetti, Barbara Onida

Dipartimento di Scienza Applicata e Tecnologia, Politecnico di Torino, Corso Duca Degli Abruzzi, 24, 10129, Torino, Italy

ARTICLE INFO

Keywords:
Drug release
Drug carrier
Hybrid
Silica
Vitamin D
Mesostructured
Mesostructure order

ABSTRACT

Vitamin D (VD) suffers from low water solubility and strong degradation, which both decrease its bioavailability. This work aims at obtaining a silica-surfactant-VD hybrid material and verifying if this system can protect VD from degradation and enhance its solubility. This preliminary study aspires at tuning the mesostructure order of the hybrid system (by modifying the surfactant amount) with the scope of controlling, somewhat, its drug release capability. To this purpose, two silica-surfactant-VD systems with different long-range order were synthesized and characterized in terms of physico-chemical properties and release behavior in a model solution mimicking the topical environment. Results show that the hybrid materials are able to incorporate VD, protect it from degradation up to 17 months and release it in aqueous media. The mesostructure order and the interaction between VD, surfactant and silica seem to play a key role in tuning kinetics and the amount of released drug. While the less ordered structure incorporates less VD with faster and higher release percentage, the more ordered one incorporates more VD but, due to the stronger interactions with the carrier, requires a partial dissolution of the matrix to occur before releasing the drug, so inducing a lag-time and a smaller released quantity.

1. Introduction

"In all things of nature there is something of the marvelous" as Aristotele said (from "Parts of Animals", book I, 645a.16). Hybrid materials available in nature make no exception. As an example, bone and nacre, which are natural hybrid materials made of a protein matrix and a mineralized inorganic component, achieve strength and toughness at the same time despite their low density [1,2]. This set of properties is desirable for technical applications and, for example, several studies on the production of synthetic nacre are present in the literature [3,4]. In general, hybrid materials have attracted growing scientific interest in the last years [5]. These systems, in fact, combine two (or more) individual components into a single structure, which results in a final material with properties that are intermediate between those of the constituents while, in some cases, a synergic effect can also be obtained.

As far as drug delivery is concerned, hybrid materials also represent the new frontier of advance towards the development of multifunctional systems [6]. In particular, the present work is focused on hybrid materials for topical drug delivery. A recent work from our research group proposed the use of a hybrid silica-surfactant carrier to deliver curcumin, an active principle potentially promising for the treatment of some skin disorders, but with the drawback of a very limited water solubility and bioavailability. In that specific study, the presence of a surfactant in the hybrid carrier allowed the curcumin solubility in water to be increased [7]. A strength of this

* Corresponding author.
E-mail addresses: marta.gallo@polito.it (M. Gallo), mauro.banchero@polito.it (M. Banchero), vittoriacerbella16@gmail.com (V. Cerbella), silvia.ronchetti@polito.it (S. Ronchetti), barbara.onida@polito.it (B. Onida).

https://doi.org/10.1016/j.heliyon.2024.e36080
Received 21 November 2023; Received in revised form 1 August 2024; Accepted 8 August 2024
Available online 14 August 2024

type of hybrids resides in the fact that they are synthesized with a one-pot process without recurring to several consecutive steps such as carrier synthesis, surfactant removal, drug loading (as reported, for example, in Refs. [8–10]). Moreover, in similar works where silica-surfactant hybrids are studied, such as those proposed by Tsai, Zheng and Meng [9,11,12], the synthesis procedures are considerably longer than ours (with ageing ranging from 24h to 5d compared to 3h of our work) and imply long energy-consuming heating steps (from 40 °C to 80 °C compared to no heating in our work). Finally, another advantage of the proposed system is related to the possible release of silicic acid from the inorganic component of the carrier, which could be beneficial to the healthy renewal of skin [13].

The present work is mainly aimed at enlarging the study of such a hybrid system, by exploring, through preliminary research, the possibility to extend its application to other active principles. Vitamin D (cholecalciferol) was here selected because of its efficacy in treating the symptoms of skin pathologies, such as psoriasis. However, vitamin D (VD) has poor water solubility and easily undergoes oxidative, thermal and light degradation [14–17]. These drawbacks are common to many active principles, as testified by the scientific effort devoted to conceive carriers able to mitigate them (e.g., lipid formulations, polymeric systems, mesoporous and aerogel silica … [18–21]). Fast degradation raises particular concern for those compounds that are conceived for topical applications, since the drug, laying on the skin surface, is exposed to oxygen and light for prolonged time. This high susceptibility to degradation of VD as well as its limited water solubility require an appropriate carrier to be employed, which makes it a suitable candidate to test the above-cited hybrid system. The proposed hybrid material, in fact, is expected to protect VD from degradation and to increase its solubility at the same time, thanks to the presence of the surfactant. To the authors' knowledge, there are no previous studies on silica-surfactant-VD hybrid systems in the literature.

Another novel and crucial topic addressed in this work is the relationship between the amount of surfactant in the hybrid and the consequent degree of mesostructure order of the carrier, which finally affects the drug release performance. As it was previously explained [7], cetyltrimethylammonium bromide (CTAB) was selected as a model surfactant even though it is cytotoxic at high concentration (a decrease in cell viability is observed in solutions with CTAB concentration of some tens of nM [22–24]. Despite this drawback, however, this surfactant is widely studied, and its phase diagram is well known. Furthermore, it is employed in synthesis processes of mesostructured silica that are robust and reproducible, which is fundamental to understand its role in the structure of the hybrid at this early stage of research. Thanks to its self-assembly properties, it can be used as a model templating agent to direct the condensation of silica in structures that are ordered at the mesoscale (i.e., mesostructured silica). As it is well-known from the water/CTAB phase diagram [25], when the CTAB content in solution increases at a given temperature, different phases, such as the hexagonal, lamellar or cubic one, can be obtained and by changing the molar ratio of the surfactant, it is consequently possible to obtain mesostructured silica with hexagonal, cubic or lamellar structure. For example, Luo and co-authors, managed to obtain silica nanoparticles with different phases by changing the molar ratio of ethanol and surfactant [26]. On the contrary, for the sake of the environment, the use of organic solvents was avoided during the synthesis of the hybrid carrier proposed by our research group and a water-based process was rather preferred. As a consequence, to change the order of the mesostructure, different molar ratios of CTAB and silica precursor (TEOS) were explored, instead of leaning on the molar ratio with ethanol. In addition, since the aim of the work is to exploit the potentialities of hybrid materials, contrary to what is usually done, the surfactant was not removed at the end of the synthesis step but was maintained as a part of the final system since it is essential to increase the solubility of the incorporated active principle. In detail, by changing the CTAB:TEOS molar ratio (from 0.122 to 0.800), two mesostructured silica-CTA hybrids with hexagonal symmetry but different degree of order could be obtained. Keeping constant the two identified molar ratios (0.122 and 0.800), VD was added to the synthesis so obtaining two silica-CTA-VD hybrids.

The above discussion has pointed out the main objectives of the present study, which can be summarized as follows: i) to prepare, for the first time, a silica-surfactant-VD hybrid, ii) to ascertain if such hybrid is able to protect VD from degradation and enhance its release in aqueous media, iii) to tailor the hybrid mesostructure order and, as a consequence, its drug release capability by tuning the amount of surfactant. In order to pursue these goals, all the synthesized samples were analyzed in terms of physico-chemical properties, their release behavior was monitored in pseudo-physiological fluids and their capacity to preserve VD from degradation was verified after some months of storage.

2. Materials and methods

2.1. Synthesis procedures

Mesostructured hybrid particles were synthesized adapting a process reported in a previous work regarding curcumin-containing hybrid carriers [7] and inspired by the literature [27,28]. This process was chosen because it does not require any heating and it makes use of mild conditions in water-based solutions, without any polluting organic solvents. As a consequence, this synthesis can be applied also to thermally and chemically unstable molecules (such as VD). All reagents were purchased from Sigma-Aldrich (Milano, Italy) and used as received.

For the synthesis of the silica-CTA-VD hybrid particles with higher order (HO_VD, High Order with Vitamin D), a procedure A was followed. It consisted in mixing 0.40 g of hexadecyltrimethylammonium bromide (CTAB) under constant stirring (300 rpm) with a 0.05 M solution of NaOH (0.19 g of NaOH in 95 mL of distilled water). After 20 min, VD was added (69 mg) and solubilized for 5 min. Afterwards, 2 mL of tetraethyl orthosilicate (TEOS) were poured dropwise. The solution, which had turned opalescent, was left under stirring (150 rpm) for 3 h at room temperature. Then the precipitate was filtered, washed with distilled water, let dry in oven at 40 °C overnight and ground.

For the silica-CTA-VD hybrid particles with lower order (LO_VD, Low Order with Vitamin D), a procedure B was followed.

Procedure B differs from procedure A for the CTAB amount, which was increased to 2.6 g and the filtration step, which was replaced by centrifugation. In particular, in procedure B, the synthesis solution was centrifuged at 4000 rpm for 15 min, washed with water, centrifuged at 4000 rpm for another 10 min, washed with water and, finally, washed with an EtOH/water solution (10/90 %vol) to remove all the unreacted CTAB.

The molar ratios in the syntheses of the hybrid materials with the higher (HO_VD) and the lower (LO_VD) order were, respectively.

- synthesis A, HO_VD: 1 TEOS:0.122 CTAB:0.536 NaOH:0.02 VD:589 H_2O
- synthesis B, LO_VD: 1 TEOS:0.800 CTAB:0.536 NaOH:0.02 VD:589 H_2O

Reference silica-CTA hybrid particles were synthesized following procedure A and B, but without adding VD in the synthesis solution. Reference samples are here identified as HO_ref and LO_ref, respectively.

The final masses of the different samples were around 0.60–0.70 g for HO_VD and HO_ref and around 1.1–1.2 g for LO_VD and LO_ref.

All samples were stored in a box, in transparent plastic vials, at room temperature.

2.2. Characterisation

Thermogravimetric (TGA) analyses were carried out using a Setaram TGA 92 (Caluire, France) by heating the samples between 20 °C and 800 °C with a heating rate of 10 °C/min in air flow.

X-Ray diffraction (XRD) data were collected using a Panalytical X'Pert PRO (Cu Kα radiation, Malvern Panalytical, Almelo, The Neatherlands), at 40 kV and 40 mA, with a solid-state detector (PIXcel1D).

Measurements were performed at low and high angles ($2\theta = 0.7°–10°$ and $2\theta = 5°–60°$, respectively). Samples, in powder form, were located in a sample-holder and the surface was flattened by manually applying a slight pressure with a blade. Measurements were acquired without any rotation of the sample-holder stage.

Field emission scanning electron microscopy (FESEM) images were recorded with a FESEM Zeiss Merlin (Oxford Instruments, Abingdon-on-Thames, UK). A small quantity of sample, in powder form, was sprinkled on a conductive adhesive tape attached on a metallic sample-holder. Before analysis, specimens were Pt-metallized.

Transmission electron microscopy (TEM) images were acquired with a Talos F200x-G2 instrument (Thermo Fischer Scientific, Waltham, MA, US). A small quantity of sample, in powder form, was dispersed in 2-propanol and sonicated for 5 s. A drop of the so-obtained dispersion was deposited on a carbon film supported on a copper grid. Analyses were carried out at 200 kV, in bright field and with an objective opening of 10–30 μm.

FTIR spectra were recorded at a resolution of 2 cm^{-1} on pelletized powders mixed with KBr using an Equinox 55 spectrometer (Bruker, Billerica, MA, USA) after outgassing the sample at room temperature (residual pressure of 0.1 Pa).

2.3. Immersion tests

Samples underwent immersion tests into two different media, ethanol (EtOH) and artificial sweat (AS), to determine the amount and the kinetics of release of the vitamin. Both immersion media were subjected to UV absorption analysis and spectra were recorded using a Lambda 25 spectrophotometer (PerkinElmer, Waltham, MA, USA). To quantify the VD content in the media, calibration curves were obtained by preparing solutions with known concentration of VD in either EtOH or AS.

Immersion tests in EtOH were conducted by immersing the samples in the solvent in static conditions; at fixed time-points (up to 3 h) an aliquot of the solution was filtered and analyzed in the 190–600 nm wavelength range. To assure a complete release of VD, at the end of the test (after 3 h) the solution was sonicated for 30 s, filtered and analyzed again.

The samples were also subjected to immersion tests in AS. The AS solution was prepared according to the literature [29] by dissolving 1.314 g NaCl, 0.075 g $CaCl_2$, 0.054 g $MgSO_4$, 0.459 g KH_2PO_4 in 450 g of distilled water and adjusting the pH to the value of 5.4

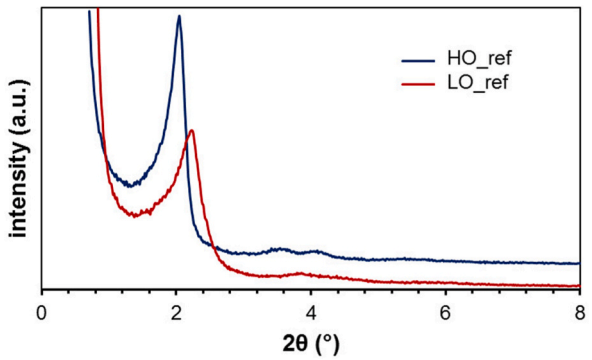

Fig. 1. XRD patterns at low angles of HO_ref and LO_ref hybrid materials.

b y adding a 0.05 M NaOH solution. 36.6 mg of HO_VD and 63.3 mg of LO_VD were separately immersed in 450 mL of AS in an Erweka DT tester (Erweka, Langen, Germany) at 32 °C under stirring (100 rpm) for 20 h. A peristaltic pump guaranteed a constant flow of solution in the spectrophotomer chamber, allowing the UV absorption at 290 nm (where the absorption peak of VD in AS is located) to be continuously recorded. At the end of the test, the solutions were filtered, and their UV/Vis-spectra were recorded in the 190–600 nm wavelength range.

3. Results and discussion

3.1. Characterization of the mesostructure order of the hybrid materials

3.1.1. Structure characterization of reference materials by means of XRD

First of all, reference samples were analyzed in order to verify the influence of the different surfactant content in the synthesis batch on the final mesostructure. Fig. 1 reports the XRD diffraction patterns at low angles of HO_ref and LO_ref materials. The HO_ref sample is characterized by a well-defined pattern with three peaks at 2θ values of 2.0, 3.5 and 4.1, which correspond to the reflections (100), (110) and (200) typical of the 2D hexagonal symmetry [30]. This is in accordance with previous results obtained for materials prepared with the same synthesis procedure [7].

The LO_ref sample, obtained with a higher surfactant content in the synthesis batch, still presents a pattern which can be assigned to the hexagonal symmetry, but the main peak (reflection (100)) is broader whereas the other reflections are barely visible, so suggesting a lower degree of order of the mesostructure. The location of the main peak, moreover, is shifted at higher 2θ values (2.3), coherently with what reported by Melendez and coauthors [31] who observed a shift of the main peak towards higher 2θ values when the ratio CTAB/TEOS was increased from 0.1 to 0.19. This effect, which indicates a smaller unit cell, was attributed to an excess of surfactant that results into a hindering of the unit cell growth and a lower extent of silica polymerization.

Given the above-observed effect of the amount of surfactant on the structure order of the hybrid reference materials, the same syntheses were repeated with the addition of VD. The samples named HO_VD (synthesis A) and LO_VD (synthesis B) were obtained and their characteristics are presented in the following sections.

3.1.2. Assessment of VD content by means of TGA and extraction tests in ethanol

Fig. 2 reports the thermogravimetric analyses of all hybrid materials and of pure VD as a comparison. All samples present an initial mass loss below 150 °C due to physisorbed water, followed by a large mass loss between 150 °C and 350 °C. In the reference samples, HO_ref and LO_ref, this mass loss is attributed to the degradation of the surfactant, which is reported to occur in the 150–300 °C range [32]. It is worth nothing that, coherently with the higher CTAB content in the synthesis batch, LO_ref (Fig. 2B) presents a higher weight loss than HO_ref (Fig. 2A).

In the VD-containing hybrid materials, HO_VD and LO_VD, the mass loss can be attributed to the degradation of both the surfactant and VD, since pure VD presents a maximum rate of degradation at around 330 °C (Fig. 2). When compared to the respective reference, both VD-containing materials present a higher mass loss, which can be ascribed to VD. In summary, the mass losses between 150 °C and 800 °C are the following: 57 wt% for HO_ref, 72 wt% for HO_VD, 60 wt% for LO_ref, 67 wt% for LO_VD (Table 1).

In order to quantify the amount of VD in HO_VD and HD_VD, extraction tests in ethanol were carried out. The so obtained solutions present a peak of absorbance due to VD at a wavelength of 265 nm (Fig. S1), coherently with the literature [33]. The absorbance value at 265 nm was converted into the concentration of VD in EtOH through a calibration curve. This allowed the amount of VD released from the sample and, therefore, the initial VD content of the hybrid to be calculated. Finally, the incorporation efficiency (IE, eq. (2)) was calculated dividing the actual amount of VD incorporated in the sample (as obtained through the immersion in EtOH) by the amount of VD introduced in the synthesis batch.

$$\mathrm{IE} = \mathrm{VD\ incorporated\ (mg)} \,/\, \mathrm{VD\ used\ in\ synthesis\ (mg)} \cdot 100, \tag{1}$$

The so obtained values of VD content and incorporation efficiency are listed in Table 1. The IE results are considerably high, above all in the HO_VD system, so proving that this kind of synthesis allows the drug loss to be limited.

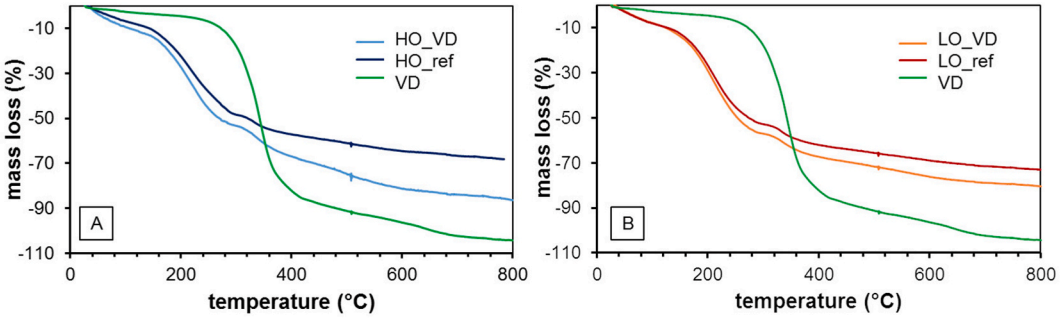

Fig. 2. TGA of HO_VD and HO_ref (A), and LO_VD and LO_ref (B). Pure VD is also reported for comparison.

Table 1
mass losses, VD content and efficiency of incorporation of VD in the hybrid materials.

sample	mass loss 150–800 °C (wt.%) from TGA	VD content (wt.%) from EtOH test	efficiency of incorporation (%) from EtOH test
HO_ref	57	–	–
HO_VD	72	8.6	90
LO_ref	60	–	–
LO_VD	67	4.1	68

It is worth noting that, if the difference in mass loss between the VD-containing samples and their references (Table 1) are compared, this is coherent with the VD content measured by the immersion test in EtOH. HO_VD, which is the sample with the highest VD content (8.6 %), presents the highest difference in mass loss when compared to the reference HO_ref (72%–57 % = 15 %). LO_VD, instead, presents both a lower VD content (4.1 %) and a smaller difference in weight loss with respect to the reference LO_ref (67%–60 % = 7 %). It must be remembered, however, that the mass loss of the samples does not depend only on the VD content, but also on the amount of surfactant present in the hybrid material.

For sake of completeness, the immersion tests of HO_VD in EtOH was repeated after a 17-month storage period in transparent vials located in a closed opaque box at room temperature. The UV–Vis spectrum obtained after 17 months is comparable to that of the newly prepared sample (Fig. S2). This indicates that the released molecule (i.e., VD) was not altered during this long storage period, suggesting that the hybrid system is able to protect VD from degradation.

3.1.3. Structure characterization of VD-containing materials by means of XRD

XRD analyses allowed the influence of the addition of VD on the structure of the hybrid materials to be investigated (Fig. 3).

The main peak of HO_VD (100) appears shifted towards higher angles with respect to that of HO_ref, so indicating a smaller hexagonal unit cell in the presence of VD (Fig. 3A). This observation can provide information about the possible location of VD in the HO_VD sample. It must be remembered, in fact, that the formation of different structures by self-assembly (cubic, hexagonal, lamellar) depends on a specific value of the surfactant molecular packing ratio (*g*). In particular, the hexagonal phase is associated with a *g* value of ½ [30]. According to the literature [34], *g* is directly proportional to the total volume of the hydrocarbon chains (*V*) and inversely proportional both to the effective area of the polar head (a_0) and the effective length of the surfactant chain (*l*):

$$g = V \,/\, (a_0 \cdot l), \tag{2}$$

The XRD patterns in Fig. 3A prove that the hexagonal phase of the reference sample (HO_ref) is maintained also in presence of VD (HO_VD), which means that *g* is constant and equal to ½. On the other hand, the shift of the XRD peaks towards higher angles and the consequent reduction of the cell parameter reflect a reduction of *l*, the effective length of the surfactant chains. As a consequence (eq. (2)), by assuming that *V* is nearly constant, in order to maintain $g = ½$ it is necessary that a_0 increases, which can be explained by the interposition of VD between the polar heads. Therefore, according to the experimental evidence given by the XRD patterns, it can be concluded that in the HO_VD hybrid material the vitamin interposes among the polar heads of CTA, probably acting as a co-surfactant.

As far as the less ordered system is concerned, the opposite phenomenon can be observed when LO_VD and LO_ref are compared (Fig. 3B). The main peak of LO_VD is shifted towards lower angles with respect to that of LO_ref, so indicating a larger unit cell and suggesting that this swelling is due to the location of VD among the hydrophobic tails of the surfactant.

Finally, it is worth mentioning that pure VD is crystalline [35]. However, the XRD patterns at high angles of both HO_VD and LO_VD (data not shown) display an amorphous halo, suggesting that VD is not segregated but is embedded in an amorphous system. This is an advantageous result, since active principles are more prone to dissolve when they are not in crystalline form.

3.1.4. Morphological and structural characterization of VD-containing materials by means of electron microscopy

FESEM images (Fig. 4B) show that the addition of VD in the ordered system alters the morphology of the material, leading to the formation of particles with larger size (600–800 nm) and less homogeneous shape when compared to those of the reference HO_ref (particle size around 400 nm, Fig. 4A). However, the hexagonal symmetry typical of the reference material (Fig. 4A and [7]) is partially

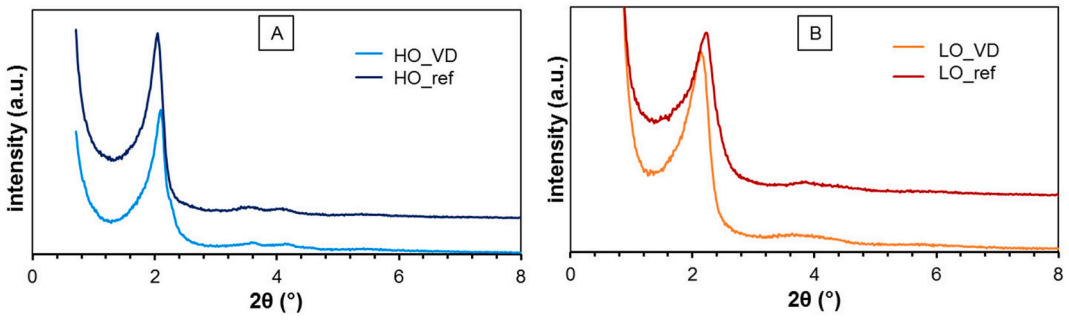

Fig. 3. XRD patterns at low angles of HO_VD and HO_ref (A), and LO_VD and LO_ref (B).

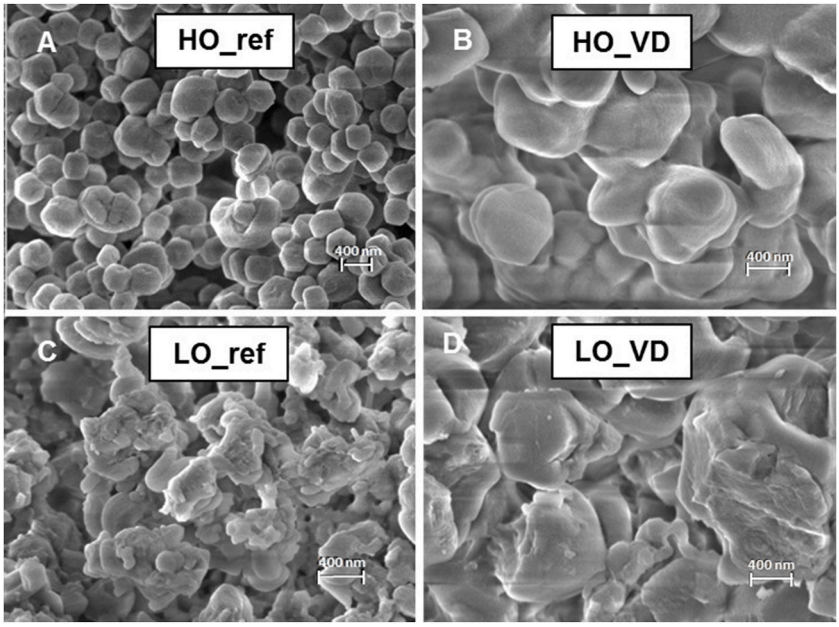

Fig. 4. FESEM images of HO_ref (A), HO_VD (B), LO_ref (C) and LO_VD (D).

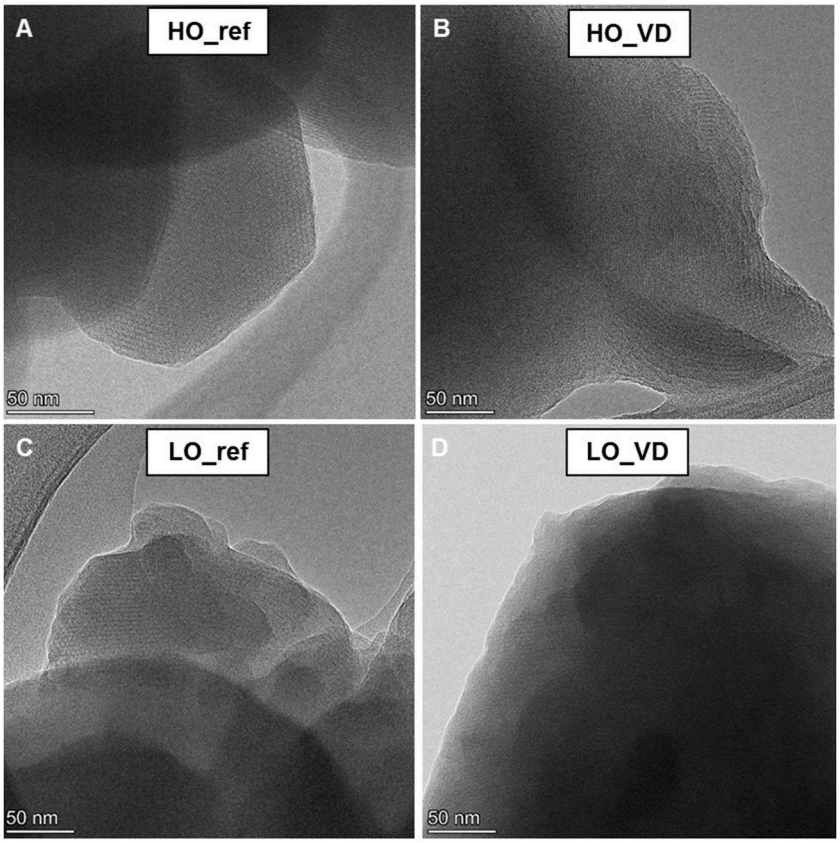

Fig. 5. TEM images of HO_ref (A), HO_VD (B), LO_ref (C) and LO_VD (D).

maintained, albeit more round. The reference less ordered material LO_ref (Fig. 4C) presents a heterogeneous and irregular morphology, which is exacerbated when VD is added (HD_VD, Fig. 4D).

On the overall, it can be concluded that the addition of both surfactant and VD in the synthesis batch affects the morphology of the final particles, decreasing the order. This, as far as the HO_VD sample is concerned, is further evidence that VD takes part in the self-assembly process behaving like a co-surfactant. In the LO_VD sample, instead, the addition of VD simply involves the swelling of the surfactant-silica matrix.

TEM images, reported in Fig. 5, confirmed what already observed through XRD and FESEM. The HO_ref material presents a well-ordered mesostructure, with parallel channels organized in the hexagonal symmetry typical of MCM-41 systems (Fig. 5A). In the LO_ref sample some ordered domains are still visible (Fig. 5C), although to a less extent with respect to HO_ref. When VD is added, the mesostructure becomes less ordered (especially in LO_VD, Fig. 5D) and only few small domains of parallel channels can be observed.

3.1.5. Spectroscopic characterization by means of FTIR

FTIR spectra of the hybrid samples in the 3800-2400 cm^{-1} range are reported in Fig. 6. All materials present absorption bands around 2900-2800 cm^{-1}, attributable to $–CH_2$- and $–CH_3$ groups, which can be ascribed to CTA in the case of HO_ref and LO_ref and to CTA and VD in the case of HO_VD and LO_VD [36]). In all samples, the negligible evidence of silanols (bands in the 3700-3000 cm^{-1} range) is in accordance with a direct electrostatic interaction between silica and CTA, in the $–SiO^-$ and CTA^+ form, respectively, this interaction being induced by the basic ambient of the synthesis process [37]. Also the band of hydroxyl groups typical of crystalline VD (inset in Fig. 6B, broad band between 3500 and 3000 cm^{-1}, labelled with a star) is negligible in the VD-containing materials (stars in Fig. 6A and B). This is in agreement with XRD results, which indicate that in the hybrid materials VD molecules are not organized in the crystalline structure.

3.2. The role of the mesostructure order of the hybrid samples on drug release

3.2.1. VD release tests in artificial sweat

The main goal of the study was to investigate the influence of the degree of material order on its release properties. To this purpose the HO_VD and LO_VD samples underwent immersion tests in artificial sweat (AS) and the absorbance of the solution was constantly monitored at 290 nm (wavelength of the absorption peak of VD in AS [38]).

Fig. 7A reports typical UV–Vis spectra obtained at the end of the immersion test; the peak is located at around 275 nm rather than 290 nm. This is likely due to the interaction between VD and the surfactant micelles (with which VD is released), as confirmed by the literature, where a similar behavior is reported for other molecules interacting with micelles [39,40]. Unfortunately, this shift of absorbance peak hindered a rigorous quantification of the VD concentration in AS, due to the difficulty in obtaining a reliable calibration plot.

Nevertheless, the plots of the absorbance value at 290 nm (normalized by the mass of the sample) as a function of time (Fig. 7B) evidence a significantly different trend for HO_VD and LO_VD, respectively. At the end of the test (20 h), similar values of absorbance are reached for both samples; however, it must be reminded that the VD content of the more ordered system (HO_VD) is more than double than that of the less ordered one (LO_VD) (8.6 wt% and 4.1 wt%, respectively, Table 1). The less ordered system, then, although it is less efficient in incorporating VD, releases a significantly higher percentage of its initial VD content with respect to the more ordered one. This definitely shows that the mesostructure order affects the release properties of the material, which is a crucial aspect when applications as drug carriers are conceived.

The profiles reported in Fig. 7B display a significantly different release kinetics. While the more ordered system, HO_VD, presents a lag-time of about 2 h, after which the release gradually increases, the less ordered system, LO_VD displays a nearly instantaneous release, which constantly increases in the first 10 h and then becomes almost stable. Finally, it is worth mentioning that for both HO_VD and LO_VD samples no residual material was observed at the end of the immersion tests.

3.2.2. Data regression of the release kinetics with literature models

In order to gain a deeper insight into the release kinetics, Fig. 8 reports the curves in terms of normalized absorbance, which was

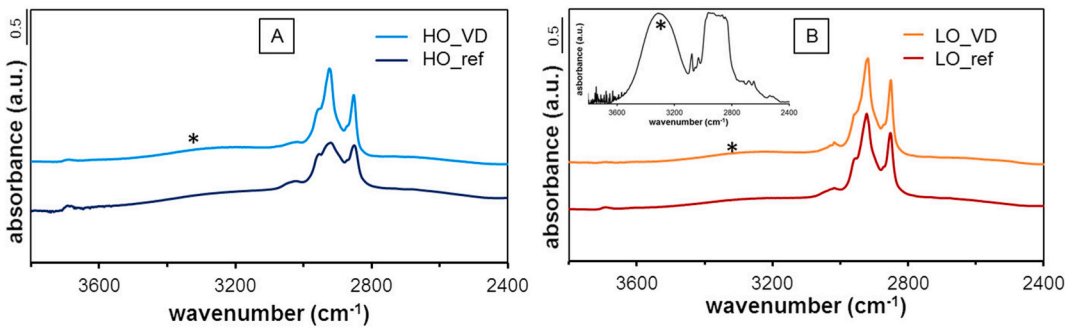

Fig. 6. FTIR spectra of HO_VD and HO_ref (A), and LO_VD and LO_ref (B). Inset in (B): FTIR spectrum of pure VD (3800-2400 cm^{-1}).

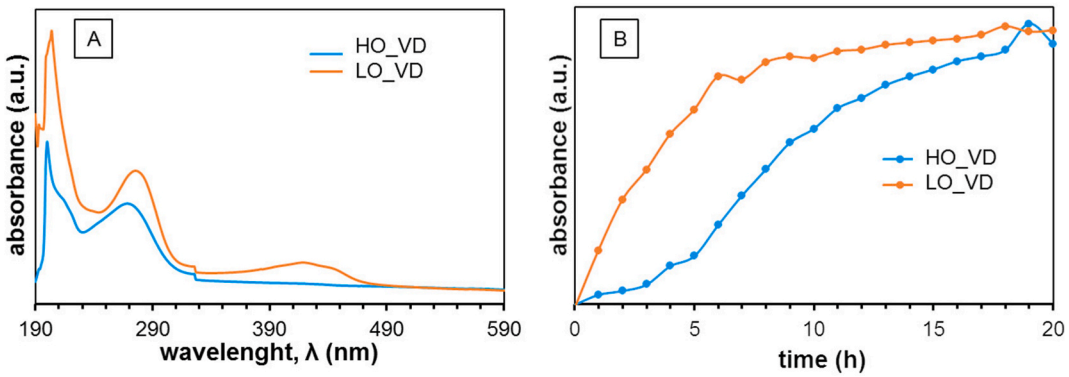

Fig. 7. Release profiles of HO_VD and HD_VD in AS.

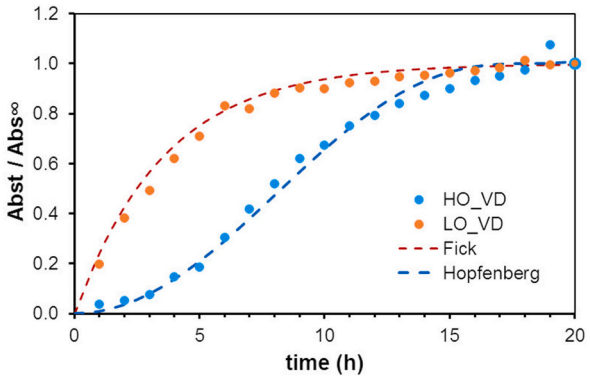

Fig. 8. Release profiles of HO_VD and HD_VD in AS and possible fitting models.

obtained by dividing the absorbance at each time "t" (Abs_t) by the absorbance at the end of the test (Abs_∞), as a function of time. The experimental data were regressed with different mathematical models in the attempt to describe the release kinetics of the hybrid systems. For sake of brevity, only the two models that best fit the experimental data are here reported.

The drug release from the LO_VD system is well fitted by a Fickian diffusion model derived from the Noyes-Whitney equation, which describes a first order kinetics and is typical of solid dosages [41]. This model is represented by the following exponential equation:

$$\frac{Abs_t}{Abs_\infty} = 1 - e^{-K_F t} \tag{3}$$

where K_F is the rate constant, which depends on solvent accessibility and its diffusion coefficient through the material [42]. Fig. 8 shows that the release kinetics of LO_VD is well described by eq. (3), with $K_F = 0.28\ h^{-1}$.

The HO_VD systems, instead, presents slower kinetics and the most satisfying fitting is obtained with a model that describes drug release from surface-eroding devices [43]. It is a modified version of that originally proposed by Hopfenberg [44] and is represented by the following equation:

$$\frac{Abs_t}{Abs_\infty} = 1 - \left(1 - K_H t^2\right)^n \tag{4}$$

where K_H is a constant depending on the erosion rate constant, the initial drug concentration in the matrix and the initial characteristic dimension of the device (i.e., the radius for spherical particles). This model can be applied to slabs, infinite cylinders and particles by simply changing the value of the exponent n ($n = 1$ for slabs, $n = 2$ for cylinders, $n = 3$ for spheres) [43]. As clearly visible in Fig. 8 the data of the HO_VD system are well regressed by eq. (4), with $n = 3$ (spherical particles) and $K_H = 0.003\ h^{-2}$.

Considering all the fitting results, the release from the LO_VD system seems to follow a first order kinetics dominated by diffusion. The HO_VD systems, instead, presents slower kinetics and the most satisfying fitting is obtained with a model that takes into account surface erosion. In particular, the release from the HO_VD sample could be governed by matrix dissolution, according to what has been previously proposed for similar curcumin-silica hybrid systems [7].

The above discussion on the different fitting of the experimental release profiles as well as the information about the location of VD

in the samples, provided by XRD (section 3.1.3), allow a possible mechanism of drug delivery for the two systems to be formulated. In the more ordered system, the VD molecules are located among the polar heads of the surfactant and, acting as co-surfactant, strongly interact with the negatively charged silica and/or with the positively charged polar heads at the interface; therefore, the release of VD requires a preliminary dissolution of the matrix to occur, as suggested by the presence of the lag-time. On the opposite, in the less ordered system, the VD molecules, being located among the CTA tails, interact only with the alkyl chains of the surfactant by means of hydrophobic interactions and can be immediately released from the material, much earlier than the matrix starts dissolving, and in higher quantity, through diffusion phenomena. This is confirmed by the absence of the lag-time. Moreover, weaker interactions between the micelles and the silica could also be considered in this case, which indeed give rise to a less ordered system by self-assembly.

In addition, it cannot be ruled out that other features, such as pore wall thickness, may play a role in affecting the release rate. Indeed, it can be supposed that the LO_VD has thinner pore walls than the HO_VD, based on the structure properties of HO_ref and LO_ref, which present different unit cell sizes. In fact, the smaller unit cell derived from the data observed for LO_ref (Fig. 1) may be ascribed to thinner pore walls due to the higher CTAB/TEOS ratio used for the synthesis, as previously reported [31].

4. Conclusions

The present work achieved to obtain CTA-silica-VD hybrid materials for the first time, showing that these systems are able to both protect the "guest" molecules from degradation up to 17 months and to release them in aqueous media. This was obtained with the model surfactant CTAB; however, the positive outcomes encourage to study, in the future, this hybrid system with new biocompatible surfactants. The present study allowed the knowledge of these hybrid systems to be deepened, showing the strong connection existing between the structure order and the release behavior. It could be observed that the amount of surfactant significantly affects the interaction between the drug and its surroundings (e.g., silica, surfactant heads …), which has consequences not only on the morphology of the resulting material, but also on its release performances. In particular, stronger interactions lead to a more ordered hybrid structure, which, on one hand, is able to incorporate more VD but, on the other, releases it in aqueous media more slowly and at a smaller extent. In fact, to release the drug, the strong interactions with the surroundings need to be broken, which is only possible when the silica matrix starts degrading. Coherently, the release curve of the ordered system can be regressed by a model that accounts for surface-erosion phenomena. On the opposite, the less ordered system, which incorporates a smaller amount of VD, is characterized by weaker interactions between the drug and the surroundings. For this reason, VD is readily released in aqueous media, displaying a kinetic behavior that can be fitted by a Fickian model based on drug diffusion.

To conclude, the amount of drug release and its kinetics can be tuned by leveraging the order of these hybrid systems, which can be achieved by simply changing the surfactant content. This characteristic makes these materials versatile for a wide variety of potential future applications ranging from those uses where fast drug release is necessary (e.g., acute diseases, wounds treatment, etc.) to those where a longer and sustained release is needed (e.g., long-term treatments for skin pathologies such as psoriasis).

Data availability statement

Data will be made available on request.

CRediT authorship contribution statement

Marta Gallo: Writing – original draft, Methodology, Investigation, Data curation, Conceptualization. **Mauro Banchero:** Writing – review & editing, Resources, Funding acquisition. **Vittoria Cerbella:** Investigation, Data curation, Conceptualization. **Silvia Ronchetti:** Validation, Resources, Funding acquisition. **Barbara Onida:** Writing – review & editing, Validation, Supervision, Resources, Methodology, Funding acquisition, Conceptualization.

Declaration of competing interest

The authors declare that they have no known competing financial interests or personal relationships that could have appeared to influence the work reported in this paper.

Appendix A. Supplementary data

Supplementary data to this article can be found online at https://doi.org/10.1016/j.heliyon.2024.e36080.

References

[1] M. Porter, J. Mckittrick, It's tough to be strong: advances in bioinspired structural ceramicbased materials, Am. Ceram. Soc. Bull. 95 (2014) 18–24.
[2] H.-L. Gao, S.-M. Chen, L. Mao, Z. Song, H.-B. Yao, H. Cölfen, X. Luo, F. Zhang, P. Zhao, Y.-F. Meng, et al., Mass production of bulk artificial nacre with excellent mechanical properties, Nat. Commun. 8 (2017), https://doi.org/10.1038/s41467-017-00392-z.

[3] H.-B. Yao, J. Ge, L.-B. Mao, Y.-X. Yan, S.-H. Yu, 25th anniversary article: artificial carbonate nanocrystals and layered structural nanocomposites inspired by nacre: synthesis, fabrication and applications, Adv. Mater. 26 (2014) 163–188, https://doi.org/10.1002/adma.201303470.

[4] M. Marcinkowska, Elaboration and Characterization of Mechanical Properties of Ceramic Composites with Controlled Architecture, Université de Lyon, 2018.

[5] G. Kickelbick, Hybrid materials – past, present and future, Hybrid. Mater. 1 (2014), https://doi.org/10.2478/hyma-2014-0001.

[6] F.U. Rehman, S. Khattak, S. Mumtaz, S. Hanif, P. Muhammad, Chapter 10 - hybrid platforms for drug delivery applications, in: S. Das, S. Thomas, P.P.B.T.-N. P. Das, D.D.A (Eds.), Woodhead Publishing Series in Biomaterials, Woodhead Publishing, 2023, pp. 217–255, https://doi.org/10.1016/B978-0-323-91376-8.00002-1. ISBN 978-0-323-91376-8.

[7] M. Gallo, F. Giudice, M. Banchero, S. Ronchetti, L. Manna, B. Onida, A mesostructured hybrid CTA–silica carrier for curcumin delivery, J. Sol. Gel Sci. Technol. 96 (2020) 236–246, https://doi.org/10.1007/s10971-020-05374-0.

[8] A.M. Kessem, M. Almukainzi, T.M. Faris, A.H. Ibrahim, W. Anwar, I.A. Elbahwy, F.R. El-Gamal, M.F. Zidan, M.A. Akl, A.M. Abd-ElGawad, A.I. Elshamy, M. Elmowafy, A pH-sensitive silica nanoparticles for colon-specific delivery and controlled release of catechin: optimization of loading efficiency and in vitro release kinetics, Eur. J. Pharm. Sci. 192 (2024) 106652, https://doi.org/10.1016/j.ejps.2023.106652.

[9] C.H. Tsai, J.L. Vivero-Escoto, I.I. Slowing, I.J. Fang, B.G. Trewyn, V.S.Y. Lin, Surfactant-assisted controlled release of hydrophobic drugs using anionic surfactant templated mesoporous silica nanoparticles, Biomaterials 32 (2011) 6234–6244, https://doi.org/10.1016/j.biomaterials.2011.04.077.

[10] L. Pasqua, F. Testa, R. Aiello, S. Cundari, J.B. Nagy, Preparation of bifunctional hybrid mesoporous silica potentially useful for drug targeting, Miroporous Meosporous Mat 103 (2007) 166–173, https://doi.org/10.1016/j.micromeso.2007.01.045.

[11] H. Zheng, C. Gao, B. Peng, M. Shu, S. Che, pH-responsive drug delivery system based on coordination bonding in a mesostructured surfactant/silica hybrid, J. Phys. Chem. C 115 (2011) 7230–7237, https://doi.org/10.1021/jp110808f.

[12] Z. Meng, C. Xue, Q. Zhang, X. Yu, K. Xi, X. Jia, Preparation of highly monodisperse hybrid silica nanospheres using a one-step emulsion reaction in aqueous solution, Langmuir 25 (14) (2009) 7879–7883, https://doi.org/10.1021/la900458b.

[13] C.D. Seaborn, F.H. Nielsen, Silicon deprivation decreases collagen formation in wounds and bone, and ornithine transaminase enzyme activity in liver, Biol. Trace Elem. Res. 89 (2002) 251–261.

[14] A. Abbasi, Z. Emam-Djomeh, M.A.E. Mousavi, D. Davoodi, Stability of vitamin D(3) encapsulated in nanoparticles of whey protein isolate, Food Chem. 143 (2014) 379–383, https://doi.org/10.1016/j.foodchem.2013.08.018.

[15] F. Mahmoodani, C.O. Perera, B. Fedrizzi, G. Abernethy, H. Chen, Degradation studies of cholecalciferol (vitamin D3) using HPLC-DAD, UHPLC-MS/MS and chemical derivatization, Food Chem. 219 (2017) 373–381, https://doi.org/10.1016/j.foodchem.2016.09.146.

[16] H. Makin, G. Jones, M. Kaufmann, M. Calverley, Analysis of vitamins D, Their Metabolites and Analogues (2010) 967–1096, https://doi.org/10.1023/b135931_11. ISBN 978-1-4020-9774-4.

[17] J. Jakobsen, P. Knuthsen, Stability of vitamin D in foodstuffs during cooking, Food Chem. 148 (2014) 170–175, https://doi.org/10.1016/j.foodchem.2013.10.043.

[18] Tomii, Y. Lipid formulation as a drug carrier for drug delivery. Curr. Pharm. Des. 8, 467–474.

[19] L.R. Asmus, R. Gurny, M. Möller, Solutions for lipophilic drugs: a biodegradable polymer acting as solvent, matrix, and carrier to solve drug delivery issues, Int. J. Artif. Organs 34 (2011) 238–242, https://doi.org/10.5301/IJAO.2011.6392.

[20] M. Gallo, L. Serpella, F. Leone, L. Manna, M. Banchero, S. Ronchetti, B. Onida, Piroxicam loading onto mesoporous silicas by supercritical CO(2) impregnation, Molecules 26 (2021), https://doi.org/10.3390/molecules26092500.

[21] M. Mohammadian, T.S. Jafarzadeh Kashi, M. Erfan, F.P. Soorbaghi, Synthesis and characterization of silica aerogel as a promising drug carrier system, J. Drug Deliv. Sci. Technol. 44 (2018) 205–212, https://doi.org/10.1016/j.jddst.2017.12.017.

[22] A. Yildirim, M. Turkaydin, B. Garipcan, M. Bayindir, Cytotoxicity of multifunctional surfactant containing capped mesoporous silica nanoparticles, RSC Adv. 6 (2016) 32060–32069, https://doi.org/10.1039/C5RA21722A.

[23] Y.P. Jia, K. Shi, J.F. Liao, J.R. Peng, Y. Hao, Y. Qu, L.J. Chen, L. Liu, X. Yuan, Z.Y. Qian, et al., Effects of cetyltrimethylammonium bromide on the toxicity of gold nanorods both in vitro and in vivo: molecular origin of cytotoxicity and inflammation, Small Methods 4 (2020) 1900799, https://doi.org/10.1002/smtd.201900799.

[24] A.M. Alkilany, P.K. Nagaria, C.R. Hexel, T.J. Shaw, C.J. Murphy, M.D. Wyatt, Cellular uptake and cytotoxicity of gold nanorods: molecular origin of cytotoxicity and surface effects, Small 5 (2009) 701–708, https://doi.org/10.1002/smll.200801546.

[25] T. Wärnheim, A. Jönsson, Phase diagrams of alkyltrimethylammonium surfactants in some polar solvents, J. Colloid Interface Sci. 125 (1988) 627–633, https://doi.org/10.1016/0021-9797(88)90030-6.

[26] L. Luo, Y. Liang, E.S. Erichsen, R. Anwander, Monodisperse mesoporous silica nanoparticles of distinct topology, J. Colloid Interface Sci. 495 (2017) 84–93, https://doi.org/10.1016/j.jcis.2017.01.107.

[27] B. Onida, B. Bonelli, L. Flora, F. Geobaldo, C.O. Arean, E. Garrone, Permeability of micelles in surfactant-containing MCM-41 silica as monitored by embedded dye molecules, Chem. Commun. (2001) 2216–2217, https://doi.org/10.1039/B105261F.

[28] Q. Cai, W.-Y. Lin, F.-S. Xiao, W.-Q. Pang, X.-H. Chen, B.-S. Zou, The preparation of highly ordered MCM-41 with extremely low surfactant concentration, Microporous Mesoporous Mater. 32 (1999) 1–15, https://doi.org/10.1016/S1387-1811(99)00082-7.

[29] T. Shimamura, T. Tairabune, T. Kogo, H. Ueda, S. Numajiri, D. Kobayashi, Y. Morimoto, Investigation of the release test method for the topical application of pharmaceutical preparations: release test of cataplasm including nonsteroidal anti-inflammatory drugs using artificial sweat, Chem. Pharm. Bull. (Tokyo). 52 (2004) 167–171, https://doi.org/10.1248/cpb.52.167.

[30] V. Meynen, P. Cool, E.F. Vansant, Verified syntheses of mesoporous materials, Microporous Mesoporous Mater. 125 (2009) 170–223, https://doi.org/10.1016/j.micromeso.2009.03.046.

[31] H.I. Meléndez-Ortiz, L.A. García-Cerda, Y. Olivares-Maldonado, G. Castruita, J.A. Mercado-Silva, Y.A. Perera-Mercado, Preparation of spherical MCM-41 molecular sieve at room temperature: influence of the synthesis conditions in the structural properties, Ceram. Int. 38 (2012) 6353–6358.

[32] J. Goworek, A. Kierys, W. Gac, A. Borówka, R. Kusak, Thermal degradation of CTAB in as-synthesized MCM-41, J. Therm. Anal. Calorim. 96 (2009) 375–382, https://doi.org/10.1007/s10973-008-9055-6.

[33] D. Arduino, Hybrid Particles for Vitamin D3 Release in View of Psoriasis Treatment, Politecnico di Torino, 2021.

[34] G. Oye, J. Sjöblom, M. Stöcker, Synthesis, characterization and potential applications of new materials in the mesoporous range, Adv. Colloid Interface Sci. 89–90 (2001) 439–466, https://doi.org/10.1016/s0001-8686(00)00066-x.

[35] F. Xia, F. Xia, H. Jin, Y. Zhao, X. Guo, Supercritical antisolvent-based technology for preparation of vitamin D3 proliposome and its characteristics, Chinese J Chem Eng 19 (6) (2011) 1039–1046, https://doi.org/10.1016/S1004-9541(11)60089-X.

[36] G. Socrates, Infrared and Raman characteristic group frequencies: tables and charts, J. Am. Chem. Soc. 124 (8) (2002) 1830, https://doi.org/10.1021/ja0153520, 3rd ed.

[37] N. Pal, A. Bhaumik, Soft templating strategies for the synthesis of mesoporous materials: inorganic, organic–inorganic hybrid and purely organic solids, Adv. Colloid Interface Sci. 189–190 (2013) 21–41, https://doi.org/10.1016/j.cis.2012.12.002.

[38] G. Palestrini, Nanoporous Silica S Drug Carrier for Vitamin D3, Politecnico di Torino, 2020.

[39] F. Giudice, Mesostructured Silica for the Release of Curcumin, Politecnico di Torino, 2019.

[40] R. Sharma, D. Jani, Interaction of cationic CTAB surfactant with curcumin, an anticarcinogenic drug: spectroscopic investigation, Tenside Surfactants Deterg 50 (2013) 283–288, https://doi.org/10.3139/113.110261.

[41] Y. Hattori, Y. Haruna, M. Otsuka, Dissolution process analysis using model-free Noyes–Whitney integral equation, Colloids Surfaces B Biointerfaces 102 (2013) 227–231, https://doi.org/10.1016/j.colsurfb.2012.08.017.

[42] E.-B. Lim, T.A. Vy, S.-W. Lee, Comparative release kinetics of small drugs (ibuprofen and acetaminophen) from multifunctional mesoporous silica nanoparticles, J. Mater. Chem. B 8 (2020) 2096–2106, https://doi.org/10.1039/c9tb02494h.
[43] P. Costa, J.M.S. Lobo, Modeling and comparison of dissolution profiles, Eur. J. Pharm. Sci. 13 (2001) 123–133.
[44] D.R. Paul, F.W. Harris, American Chemical Society Division of Organic Coatings and Plastics Chemistry, American Chemical Society Division of Polymer Chemistry American chemical society meeting (171st : 1976 : New York N.Y.), N.Y. Controlled release polymeric formulations, The Society Washington (1976), Washington SE - ix, 1976, p. 317. https://worldcat.org/title/2401698. illustrations ; 24 cm. ISBN 0841203415; 9780841203419.